COMMUNICATIONS IN COMPUTATIONAL PHYSICS
Vol. **6**, No. 2, pp. 247-268

Commun. Comput. Phys.
August 2009

Complex Transition of Double-Diffusive Convection in a Rectangular Enclosure with Height-to-Length Ratio Equal to 4: Part I

Xian Liang[1,*], Xinliang Li[2], Dexun Fu[2] and Yanwen Ma[2]

[1] *Shanghai Institute of Applied Mathematics and Mechanics, Shanghai University, No. 149 Yanchang Road, Shanghai 200072, China.*
[2] *LNM, Institute of Mechanics, Chinese Academy of Sciences, No. 15 Beisihuanxi Road, Beijing 100190, China.*

Received 2 June 2008; Accepted (in revised version) 29 August 2008

Available online 15 December 2008

Abstract. This is the first part of direct numerical simulation (DNS) of double-diffusive convection in a slim rectangular enclosure with horizontal temperature and concentration gradients. We consider the case with the thermal Rayleigh number of 10^5, the Pradtle number of 1, the Lewis number of 2, the buoyancy ratio of composition to temperature being in the range of $[0,1]$, and height-to-width aspect ration of 4. A new 7th-order upwind compact scheme was developed for approximation of convective terms, and a three-stage third-order Runge-Kutta method was employed for time advancement. Our DNS suggests that with the buoyancy ratio increasing form 0 to 1, the flow of transition is a complex series changing from the steady to periodic, chaotic, periodic, quasi-periodic, and finally back to periodic. There are two types of periodic flow, one is simple periodic flow with single fundamental frequency (FF), and another is complex periodic flow with multiple FFs. This process is illustrated by using time-velocity histories, Fourier frequency spectrum analysis and the phase-space trajectories.

AMS subject classifications: 65Y20, 34C28, 70K50

Key words: Double diffusive convection, transition, periodic motion, chaotic motion, high order compact.

1 Introduction

Double-diffusive convection motion, as a common flow phenomena in nature, has been studied for a long time. It exists in many procedures containing multi-physics and multi-process coupling and interaction. For instance, the global ocean circulation driven by

*Corresponding author. *Email addresses:* `liangx_yan@126.com` (X. Liang), `lixl@lnm.imech.ac.cn` (X. L. Li), `fudx@lnm.imech.ac.cn` (D. X. Fu), `mayw@lnm.imech.ac.cn` (Y. W. Ma)

 ©2009 Global-Science Press

interaction of temperature and salinity, diffusion of pollution and temperature in soil contamination and atmospheric pollution, solar energy concentration, nuclear reactor cooling. Furthermore, the multi-diffusive convection exists in some special fields, such as the action of crystal growth and solidification of metallic alloys.

At present, cavity physics modeling [1–3], Boussinesq modeling [4,5] and k-ε modeling [6–8] are extensively used in investigation of the double-diffusive convection problem. It is mainly influenced by parameter set Ω (Ra_T, N, Pr, Le, A) [9], where Ra_T is the thermal Rayleigh number, N is the buoyancy ratio of composition to temperature, Pr is the Prandtl number, Le is the Lewis number (the ratio of composition to heat diffusivity) and A is the height-to-width aspect ratio. It is far too difficult to have a systematic investigation to cover all of the parameter set. For decades, researchers have investigated double-diffusive convection by choosing different parameter separately. Quon [9, 10], Lee [4,5] and Tsitverblit [13] investigated the multi-cell flow structure and multi-stratified stable region with various values of A, Le, N and different boundary conditions. Quon [9] investigated the mechanism of spontaneous, abrupt changes in thermohaline circulation in an idealized context, by using a two-dimensional Boussinesq fluid in rectangular containers with Rayleigh number up to 10^5.

The double-diffusive convection is a strong nonlinear coupled process, which contains the steady flow, the periodic flow, the quasi-periodic flow, the chaos, and even the turbulence. A similar problem, i.e., a lid-driven square cavity flow, has already been investigated for decades. Garcia [12] has proposed a comprehensive long term dynamic behavior of such problem. He observed that for low Reynolds numbers, the solution was stationary. For moderate Reynolds numbers, it was time periodic; and for high Reynolds numbers, the solution was neither stationary nor time periodic: the solution becomes chaotic. Some relevant papers about this topic can also be found in [12]. Tsitverblit and Kit [13] reported that a vertical rectangular enclosure was characterized by complex steady bifurcation phenomena, containing stably stratified brine and differentially heated from its side walls. Nishimura [11] has studied the Hopf bifurcation with various values of N by using the Galerkin finite element method. He claimed that the key mechanism for the oscillatory flow was that the unstable stratified region of species shifts from the central part of the enclosure to the upper and lower parts and vice versa in a time-periodic sense, due to the interaction of heat and mass transfer with different diffusivities near the vertical walls. Recently, Papanicolaou and Belessiotis [14] reported that the unsteadiness in the laminar-flow regime is due to interactions between the main flow cells affecting the bulk of the enclosure, whereas in the turbulent flow regime due to thermal release and motion along the bottom surface through studying the double-diffusive natural convection in an asymmetric trapezoidal enclosure. Masuda et al. [15] reported three types of peculiar oscillating convection in porous medium, called chaotic oscillations, sudden steady state and re-oscillation in their paper.

The DNS of double-diffusive convection problem has attracted considerable attentions. The rapid development of computing techniques provided powerful capacity to anatomize such complex problems, especially the complicate transition [9, 11, 14, 15] in

the flow. Even the flow in a simple geometry aspect, square or rectangular, requires a great deal of computer efforts to solve the strong nonlinear coupled system. Therefore, it is extremely important to design highly efficient numerical algorithms. At present, many numerical methods have been developed and applied to solve such flow problems based on finite difference, finite volume and finite element methods. The finite volume method and the finite element method with good conservation property have been used extensively, although accuracies are lower. The finite difference method has been extensively adopted in DNS for flow problems, such as boundary layer transition, compressible turbulence, multi-physics and multi-scale flow. The process of double-diffusive convection also includes multi-scale structures, or chaotic behaviors, which needs high order schemes to grasp as much as its minutia. Based on these requirements, high-order and high-resolution upwind compact finite difference schemes were constructed, which will be applied in the present numerical investigation.

As a basic factor of the flow in enclosure, the effects of aspect ratio A have been studied by many researches [9–11, 16–18]. Most researches choose $A \leq 2$, and a few for $A \geq 4$ [14]. So it is interesting to investigate the flow characteristics, especially the transition, in the enclosure for $A=4$. In the present paper, the buoyancy ratio, N, is varied for the rectangular enclosure of $A=4$ while other parameters are kept constant ($Ra_T=10^5$, $Pr=1$, $Le=2$). The detailed meanings of these parameters can be found in [9, 11].

This paper is organized as follows: In Section 2, the physical modeling, governing equations, boundary conditions and dimensionless parameters are introduced. In Section 3, a new method of finite difference discretization is described, together with high efficiency segregated solution algorithm. In Section 4, the results of the numerical simulations are reported, including the time-velocity histories, Fourier frequency spectrum and phase-space trajectories for N increasing from 0 to 1.

2 Problem formulation

The physical system consists of a rectangular enclosure as shown in Fig. 1. The top and bottom of the enclosure are considered to be adiabatic and impermeable to mass transfer. Moreover, uniform temperature and concentration differences are imposed across the vertical walls, where the thermal buoyancy force retards the compositional buoyancy force, i.e., opposing to flow.

The media fulled in the enclosure is the same as that used in [11]. As illustrated in Fig. 1, the left wall is a source, where the material and heat diffuse from the surface towards the bulk fluid of binary mixture, while the other vertical wall is a sink, where the material and heat diffuse from the bulk to the surface of the wall. The whole fluids in the enclosure flow move from the source to the sink continuously. The buoyancy produced by temperature difference force the fluid flow upwards. Meanwhile, the buoyancy produced by concentration difference force the fluids downwards, which is a set of complex competitive system. To simplify the problem, the fluid is considered as incompressible

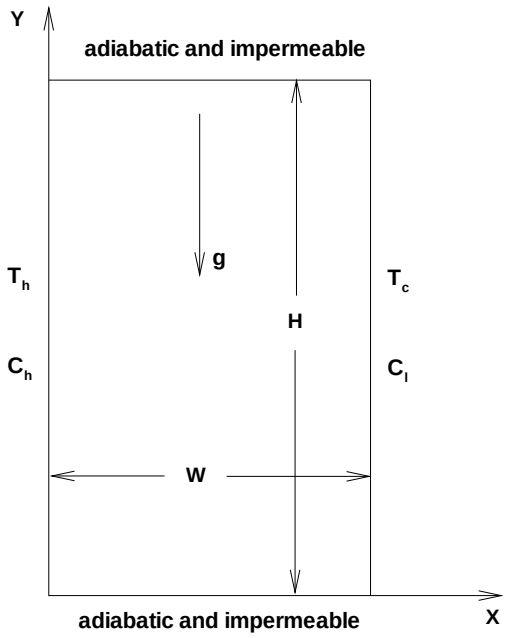

Figure 1: Enclosure flow configuration, coordinates, and boundary conditions.

and Newtonian with negligible viscous dissipations. Thermophysical properties are assumed to be independent and also Boussinesq approximation is utilized. According to the work of Quon [9], the followings are introduced, 1) a Cartesian coordinate $X=(x,y)$, 2) velocity vector $V=(u,v)$, 3) the characteristics to non-dimensionalize the equations: length scale L, the length of the enclosure, velocity scale $U=(\kappa_T\nu)^{1/2}/L$, κ_T and ν being respectively the thermal diffusivity and kinematic viscosity, (while define κ_C being the coefficient of diffusivity for the concentration), time scale $\tau=L/U$, and temperature and concentration scales ΔT and ΔC, which are respectively the maximum temperature and concentration difference in the enclosure. The governing equations that describe double-diffusive convection in terms of the streamfunction ψ, vorticity ξ, temperature T and concentration C, are given as follows

$$\psi_{xx}+\psi_{yy}=-\xi, \tag{2.1}$$

$$\xi_t+(V\cdot\nabla)\xi=Pr\nabla^2\xi+Pr\cdot Ra_T(T_x-NC_x), \tag{2.2}$$

$$T_t+(V\cdot\nabla)T=\nabla^2T, \tag{2.3}$$

$$C_t+(V\cdot\nabla)C=\nabla^2C/Le. \tag{2.4}$$

The streamfunction and vorticity are defined as

$$u=\psi_y,\quad v=-\psi_x,\quad \xi=v_x-u_y. \tag{2.5}$$

The main dimensionless parameters are

$$\begin{aligned}
&Pr=\nu/\kappa_T, \quad \text{the Prandtl number,}\\
&Ra_T=g\beta_T\triangle T\cdot L^3/\kappa_T\gamma, \quad \text{the (thermal) Rayleigh number,}\\
&Le=\kappa_C/\kappa_T, \quad \text{the Lewis number,}\\
&N=\beta_C\triangle C/\beta_T\triangle T, \quad \text{the buoyancy ratio number,}
\end{aligned}$$

which are based on the following equation of state

$$\rho=\rho_0[1-\beta_T(T-T_0)+\beta_C(C-C_0)], \tag{2.6}$$

where

$$\beta_T=-\frac{1}{\rho_0}\frac{\partial\rho}{\partial T}|_{C_0}, \quad \beta_C=-\frac{1}{\rho_0}\frac{\partial\rho}{\partial C}|_{T_0}.$$

Here T_0, C_0 and ρ_0 are reference temperature, concentration and density, respectively. The boundary conditions are

$$\begin{aligned}
&y=0 \text{ and } A: \quad u=\frac{\partial v}{\partial x}=\psi=0, \quad \xi=-\frac{\partial^2\psi}{\partial y^2}, \quad \frac{\partial T}{\partial y}=0, \quad \frac{\partial C}{\partial y}=0,\\
&x=0: \quad \frac{\partial u}{\partial y}=v=\psi=0, \quad \xi=-\frac{\partial^2\psi}{\partial x^2}, \quad T=0.5, \quad C=0.5,\\
&x=1: \quad \frac{\partial u}{\partial y}=v=\psi=0, \quad \xi=-\frac{\partial^2\psi}{\partial x^2}, \quad T=-0.5, \quad C=-0.5.
\end{aligned}$$

3 Numerical method

3.1 The 7th-order upwind compact scheme (UDC7)

In this part, a new 7th-order upwind compact scheme is developed. Consider the following model equation and its semi-discrete approximation

$$\frac{\partial f}{\partial t}+c\frac{\partial f}{\partial x}=0, \quad c=\text{constant}, \tag{3.1}$$

$$\frac{\partial f_j}{\partial t}+cF_j=0, \tag{3.2}$$

where F_j is an approximation of the first derivative $\frac{\partial f}{\partial x}$. Suppose the following relations are satisfied between an unknown function $f(x)$ and its first derivative $F(x)$, on seven-node uniform stencil $x=x_{j+k}$, $(k=-3,-2,-1,0,1,2,3)$,

$$\begin{aligned}
&a_{-3}f_{j-3}+a_{-2}f_{j-2}+a_{-1}f_{j-1}+a_0f_j+a_1f_{j+1}+a_2f_{j+2}+a_3f_{j+3}\\
&\quad+\triangle x(b_{-1}F_{j-1}+a_0F_j+a_1F_{j+1})=0.
\end{aligned} \tag{3.3}$$

The relations between the coefficients a_k $(k=-3,-2,-1,0,1,2,3)$ and b_m $(m=-1,0,1)$ are derived by matching the Taylor series coefficients of various orders. The first unmatched coefficient determines the formal truncation error. Finally, the following constraining system is obtained

$$\begin{cases} a_{-3}+a_{-2}+a_{-1}+a_0+a_1+a_2+a_3=0, \\ (-3a_{-3}-2a_{-2}-a_{-1}+a_1+2a_2+3a_3)+(b_{-1}+b_0+b_1)=0, \\ (3^2a_{-3}+2^2a_{-2}+a_{-1}+a_1+2^2a_2+3^2a_3)+2(-b_{-1}+b_1)=0, \\ (-3^3a_{-3}-2^3a_{-2}-a_{-1}+a_1+2^3a_2+3^3a_3)+3(b_{-1}+b_1)=0, \\ (3^4a_{-3}+2^4a_{-2}+a_{-1}+a_1+2^4a_2+3^4a_3)+4(-b_{-1}+b_1)=0, \\ (-3^5a_{-3}-2^5a_{-2}-a_{-1}+a_1+2^5a_2+3^5a_3)+5(b_{-1}+b_1)=0, \\ (3^6a_{-3}+2^6a_{-2}+a_{-1}+a_1+2^6a_2+3^6a_3)+6(-b_{-1}+b_1)=0, \\ (-3^7a_{-3}-2^7a_{-2}-a_{-1}+a_1+2^7a_2+3^7a_3)+7(b_{-1}+b_1)=0. \end{cases} \tag{3.4}$$

There are 10 unknowns with 8 equations. The following system of fundamental solutions containing two solution vectors can be obtained:

$$\begin{cases} \lambda_1=(\frac{1}{60},-\frac{4}{15},-\frac{13}{12},\frac{8}{3},-\frac{13}{12},-\frac{4}{15},\frac{1}{60},-1,0,1), \\ \lambda_2=(-\frac{1}{120},\frac{3}{20},\frac{19}{16},-1,-\frac{3}{8},\frac{1}{20},-\frac{1}{240},\frac{3}{4},1,0). \end{cases} \tag{3.5}$$

Therefore, any solution vector (a_{-3}, a_{-2}, a_{-1}, a_0, a_1, a_2, a_3, b_{-1}, b_0, b_1) of the system (3.4) can be linearly expressed by the system of the fundamental solutions (3.5), and any solution vector can formulate a 7th-order compact scheme. With the requirement

$$b_{-1}+b_0+b_1=1, \tag{3.6}$$

the following 7th-order upwind compact scheme with one free parameter, α, can be obtained through linear combination of λ_1 and λ_2 as $-\alpha\lambda_1+\frac{4}{7}\lambda_2$:

$$\begin{aligned} &-\alpha F_{j+1}+\frac{4}{7}F_j+(\frac{3}{7}+\alpha)F_{j-1} \\ =&\frac{1}{\triangle x}\Big[(\frac{1}{210}+\frac{\alpha}{60})f_{j-3}+(-\frac{3}{35}-\frac{4\alpha}{15})f_{j-2}+(-\frac{19}{28}-\frac{13\alpha}{12})f_{j-1} \\ &+(\frac{4}{7}+\frac{8\alpha}{3})f_j+(\frac{3}{14}-\frac{13\alpha}{12})f_{j+1}+(-\frac{1}{35}-\frac{4\alpha}{15})f_{j+2}+(\frac{1}{420}+\frac{\alpha}{60})f_{j+3}\Big]. \end{aligned} \tag{3.7}$$

The principal term of the formal truncation error of (3.3) is

$$\varepsilon_{tp}=\frac{-3-14\alpha}{5880}(\triangle x)^8.$$

With the initial condition

$$f(x,0)=e^{ikx}, \tag{3.8}$$

Eq. (3.1) has exact solution

$$f(x,t)=e^{ik(x-ct)}, \tag{3.9}$$

where $i=\sqrt{-1}$. With the same initial condition Eq. (3.8), one can obtain the solution of Eq. (3.2) as

$$f(x_j,t)=e^{-\frac{k_r}{\triangle x}ct}e^{ik(x_j-c\frac{k_i}{\omega}t)}. \tag{3.10}$$

Corresponding to UDC7, the real and the imaginary parts of the modified wavenumber are given by

$$k_i(\omega)=\frac{AC+DB}{C^2+D^2}, \quad k_r(\omega)=\frac{AD-BC}{C^2+D^2}, \tag{3.11}$$

respectively, where $0\le\omega=k\triangle x\le\pi$ is the wavenumber and

$$\begin{aligned}
&A=375\sin(\omega)+24\sin(2\omega)-\sin(3\omega),\\
&B=-240-1120\alpha+(3+14\alpha)\big[65\cos(\omega)+16\cos(2\omega)-\cos(3\omega)\big],\\
&C=60(4+3\cos(\omega)), \quad D=-60(3+14\alpha)\sin(\omega).
\end{aligned}$$

With $\alpha=-\frac{3}{14}$, we have $k_r(\omega)=0$ and $\varepsilon_{tp}=0$. Consequently, (3.7) is the 8th-order-accurate symmetrical compact difference (SCD8) approximation. Suppose $c>0$ in (3.1). $k_r(\omega)$ with $-\frac{3}{14}<\alpha<0$ is positive and the scheme (3.2) is dissipative. The following simplest 7th-order dissipative (or upwind) compact (UDC7) approximation can be obtained if $\alpha=0$ is taken

$$\begin{aligned}
&\frac{4}{7}F_j+\frac{3}{7}F_{j-1}\\
=&\frac{1}{\triangle x}\Big[\frac{1}{210}f_{j-3}-\frac{3}{35}f_{j-2}-\frac{19}{28}f_{j-1}+\frac{4}{7}f_j+\frac{3}{14}f_{j+1}-\frac{1}{35}f_{j+2}+\frac{1}{420}f_{j+3}\Big].
\end{aligned} \tag{3.12}$$

Fig. 2 shows the numerical wavenumber for different compact upwind finite difference schemes, in which UDC7, UDC5,UDC3 denote the present 7th-order, 5th-order [22] and 3rd-order [23] upwind compact schemes, respectively. It is observed that the present 7th-order scheme has higher resolution. Moreover, Fig. 2(b) shows that UDC7 is a dissipative scheme, which is helpful to depress high-wavenumber numerical oscillation. Therefore, UDC7 is appropriate for discretizing the nonlinear convective terms in the governing equations (2.1)-(2.4).

3.2 Discretization of governing equations

We will consider the streamfunction-vorticity formulation, which avoids solving the pressure poisson equation. We first design high-order upwind compact schemes to approximate the nonlinear terms. It is noticed that the governing equations (2.2)-(2.4) can be written in a unified form:

$$\frac{\partial f}{\partial t}+u\frac{\partial f}{\partial x}+v\frac{\partial f}{\partial y}=a(\frac{\partial^2 f}{\partial x^2}+\frac{\partial^2 f}{\partial y^2})+Q, \tag{3.13}$$

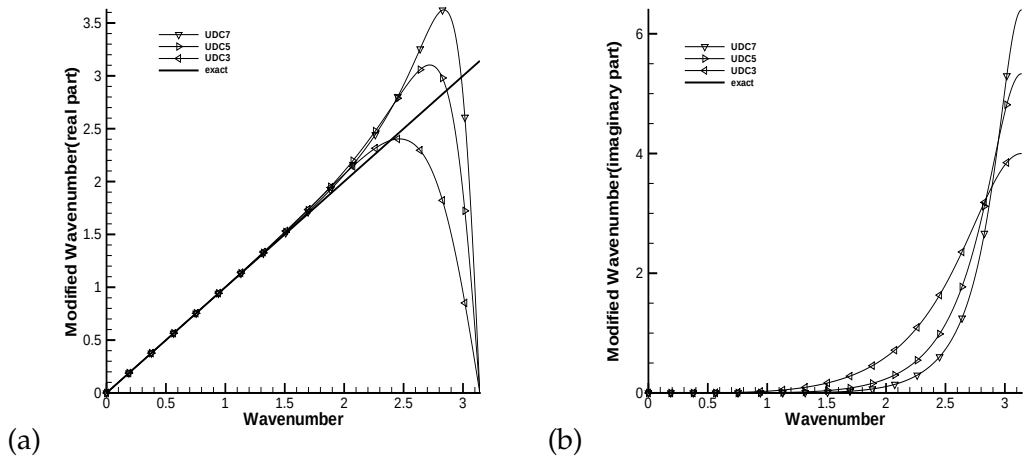

Figure 2: Modified wavenumber: (a) real part; (b) imaginary part.

where f can respectively denote vorticity, temperature, and concentration, and Q is the source term. The term $u\frac{\partial f}{\partial x}$ is computed by UDC7 in two cases. In the case of $u>0$, the term $\frac{\partial f}{\partial x}$ is approximated by F^+ with

$$\begin{aligned}&\frac{4}{7}F_j^+ + \frac{3}{7}F_{j-1}^+\\ =&\frac{1}{\triangle x}\Big[\frac{1}{210}f_{j-3}-\frac{3}{35}f_{j-2}-\frac{19}{28}f_{j-1}+\frac{4}{7}f_j+\frac{3}{14}f_{j+1}-\frac{1}{35}f_{j+2}+\frac{1}{420}f_{j+3}\Big],\end{aligned} \tag{3.14}$$

while in the case of $u<0$, the term $\frac{\partial f}{\partial x}$ is approximated by F^- with

$$\begin{aligned}&\frac{3}{7}F_{j+1}^- + \frac{4}{7}F_j^-\\ =&\frac{1}{\triangle x}\Big[-\frac{1}{420}f_{j-3}+\frac{1}{35}f_{j-2}-\frac{3}{14}f_{j-1}-\frac{4}{7}f_j+\frac{19}{28}f_{j+1}+\frac{3}{35}f_{j+2}-\frac{1}{210}f_{j+3}\Big].\end{aligned} \tag{3.15}$$

The diffusive terms are discretized using the sixth-order-accurate symmetrical compact difference (SCD6) [19]. Typically, $\frac{\partial^2 f}{\partial x^2}$, denoted by S, is discretized by

$$\frac{1}{12}S_{j-1}+\frac{5}{6}S_j+\frac{1}{12}S_{j+1}=\frac{1}{\triangle x^2}\Big[12(f_{j-1}-2f_j+f_{j+1})+\frac{3}{4}(f_{j-2}-2f_j+f_{j+2})\Big]. \tag{3.16}$$

Of course the SCD8 (for $\alpha=-\frac{3}{14}$ in (3.7)) can be used to approximate the diffusive terms, which is regarded as a suitable substitution for SCD6 here.

Suppose all spacial derivatives in Eq. (3.13) are discretized. Then a semi-discretized approximation for (3.13) is obtained

$$\frac{df}{dt}=\mathbb{L}(f). \tag{3.17}$$

A three-stage Runge-Kutta (R-K) method with third-order accuracy [20] is used to discretize the resulting ordinary differential equations:

$$\begin{aligned} f^{(1)} &= f^n + \triangle t \mathbb{L}(f^n), \\ f^{(2)} &= \frac{3}{4} f^n + \frac{1}{4} f^{(1)} + \frac{1}{4} \triangle t \mathbb{L}(f^{(1)}), \\ f^{n+1} &= \frac{1}{3} f^n + \frac{2}{3} f^{(2)} + \frac{2}{3} \triangle t \mathbb{L}(f^{(2)}), \end{aligned} \tag{3.18}$$

where

$$\mathbb{L}(f) \equiv -u\frac{\partial f}{\partial x} - v\frac{\partial f}{\partial y} + a(\frac{\partial^2 f}{\partial x^2} + \frac{\partial^2 f}{\partial y^2}) + Q. \tag{3.19}$$

In the neighborhood of all boundaries, smooth transition from the high-order schemes used in the interior of the computational domain to a third-order scheme for convection terms and fourth-order scheme for viscous terms are utilized. However, this may affect the overall accuracy slightly. In the present paper, UDC5 and UDC3 are employed for approximating convection terms adjacent to the boundary. Furthermore, a fourth-order nine-point compact finite difference scheme was employed for solving the Poisson equation (2.1). Some relevant schemes can be found in [24–27], where detailed derivation of the steady incompressible Navier-Stokes equations with streamfunction-vorticity formulation can be found. Moreover, some high-order biased difference schemes [19] were used for approximation of boundary points, see also [21,24–27].

We compared the present finite difference solutions with spectral solutions [28] and finite element solutions [11] to confirm the numerical accuracy and efficiency. Table 1 compares some relevant results of dimensionless periodic of oscillation, τ_0; stream function extremum, $|\psi_{max}|$ and $|\psi_{min}|$, which indicate the strength of thermal and compositional recirculations. The good agreement confirms the validation of present numerical method and code.

Table 1: Comparison between the different numerical methods for $Ra_T = 10^5$, $Pr = 1$, $Le = 2$, $N = 1$, and $A = 2$.

	Finite difference method (31×41) Present	Finite element method (31×41) [11]	Spectral method (40×80) [28]
τ_0	0.0489	0.0497	0.0494
$Max\|\psi_{max}\|$	26.9	26.7	26.8
$Min\|\psi_{max}\|$	12.5	12.9	12.7
$Max\|\psi_{min}\|$	5.67	5.76	5.52
$Min\|\psi_{min}\|$	0.343	0.351	0.333

We also carried out grid refinement tests. A typical case with $Ra_T = 10^5$, $Pr = 1$, $Le = 2$, $N = 0.8$, and $A = 4$ was computed with grids 16×61, 31×121 and 61×241, respectively. The test results of mean Nusselt number

$$\overline{Nu} = \frac{1}{A}\int_0^A (\frac{\partial T}{\partial x})_{x=0} dy \tag{3.20}$$

and the mean Sherwood number

$$\overline{Sh}=\frac{1}{A}\int_0^A(\frac{\partial C}{\partial x})_{x=0}dy \tag{3.21}$$

along the hot (high concentration) wall, maximum velocities u_{max} and v_{max}, the ψ_{max} and ψ_{min} in the whole fields are listed in Table 2. The solution on the mesh 31×121 is very close to the ones obtained on the finest mesh 61×241. It is believed that the mesh 31×121 is appropriate in the present computations. Since the CPU time for computing the enclosure on the 61×241 grids is more than 4 times of that for the 31×121 grids and the study on the complex transition requires very large computational efforts, we then adopt the 31×121 mesh system in the present investigation. Time steps of the order of 10^{-5} were used.

Table 2: Grid-dependence of double-diffusive convection for $Ra_T=10^5$, $Pr=1$, $Le=2$, $N=0.8$, and $A=4$.

$grid$	$\overline{Nu}$	$\overline{Sh}$	u_{max}	v_{max}	ψ_{max}	ψ_{min}
16×61	2.9522	2.4783	47.2096	128.6440	0.00001	-33.9940
31×121	2.8157	2.7097	47.8136	126.8233	0.00310	-33.4439
61×241	2.8290	2.7749	48.1120	127.1935	0.00419	-33.5561

4 Numerical results

In this paper, the buoyancy ratio N, is varied for the rectangular enclosure of $A=4$ while other parameters are kept constant, i.e., $Ra_T=10^5$, $Pr=1$ and $Le=2$. The detailed analysis for the thermophysics can be found in [11, 29]. Some useful results and irradiative phenomena are mainly presented through numerical simulations. The time-evolution of the velocity, the Fourier frequency spectrum analysis and the phase trajectory on u-v plane are shown at a fixed point $(x,y)=(0.25,1)$ of the enclosure. All of the possible flow patterns include the steady flow, the strictly periodic flow, the quasi-periodic flow and the chaotic flow.

In our simulation, the buoyancy ratio N grows form 0 to 1 with a stepsize $\triangle N$, and there are two kinds of $\triangle N$ in computation. The first one is coarse step, $\triangle N=0.02$, and the second one is fine step, $\triangle N=0.002$. The coarse step is used firstly. If the flow pattern changes rapidly within $\triangle N$, more computations are added by using finer $\triangle N$ to decide a relatively exact transition point. The computation starts from zero initial fields for each buoyancy ratio; in other words, it is independent between different buoyancy ratio. In [11], the previous solution was used to initiate the computation of the next buoyancy ratio.

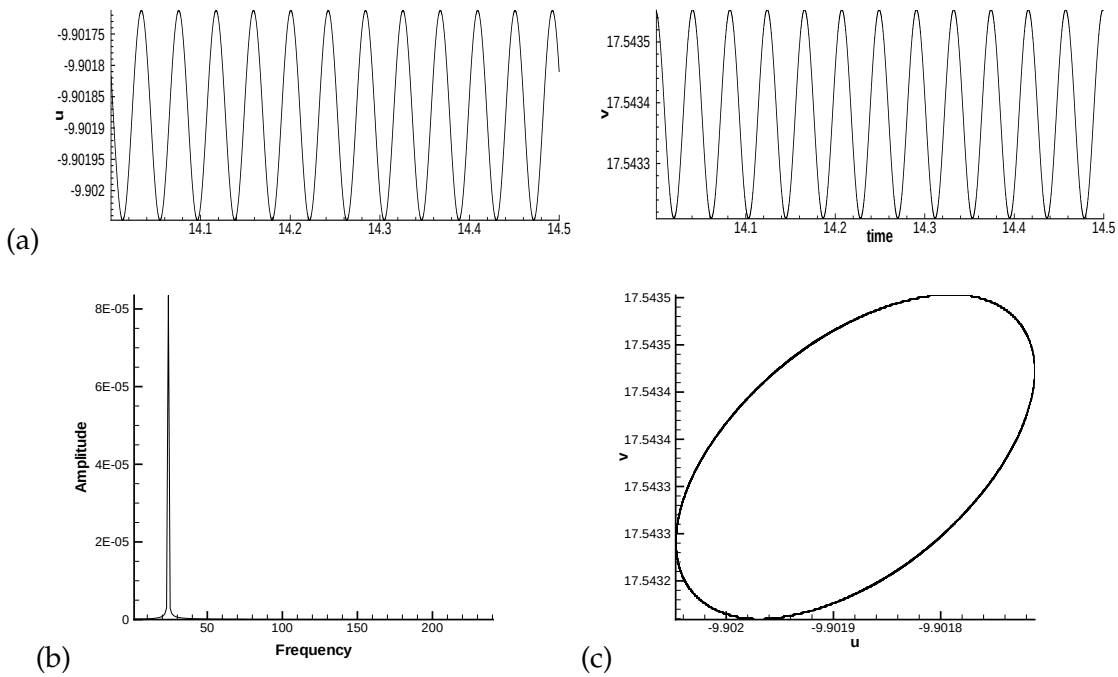

Figure 3: Computed enclosure flow at $N=0.86$. (a) u and v as a function of time; (b) Fourier frequency spectrum of the u velocity; (c) phase-space trajectories of v vs. u.

4.1 Transition process

It is found that the steady thermal-dominated flow becomes unstable via a supercritical Hopf bifurcation and changes to the periodic flow when N exceeds a threshold value. It is difficult to estimate the exact critical value of N for the underlying physical problems by numerical calculations because there exist many factors to limit this task. But a relatively small region is estimated, in which the critical N lie. Table 3 lists six critical buoyancy ratios and its approximate range in the interval $[0,1]$ obtained by the present DNS. These six values divide the interval $[0,1]$ into seven subintervals in which new flow patterns have been observed.

Table 3: The approximate position of six critical buoyancy ratio for $N\in[0,1]$.

N_1	N_{11}	N_{12}	N_{13}	N_{14}	N_{15}
(0.856,0.858)	(0.869,0.87)	(0.942,0.944)	(0.962,0.964)	(0.966,0.968)	(0.970,0.972)

It is observed that the flow is steady for $N\in(0,N_1)$. It is noted that the first Hopf bifurcation appears when $N\geq N_1$, and the periodic flow sustains for $N\in(N_1,N_{11})$. For clear visualization of the periodic flow at this interval, the time-evolution of the velocity components u and v, the phase trajectory on the u-v plane, and the Fourier frequency spectrum analysis to identify the fundamental frequency (FF) are shown in Fig. 3. Two conclusions

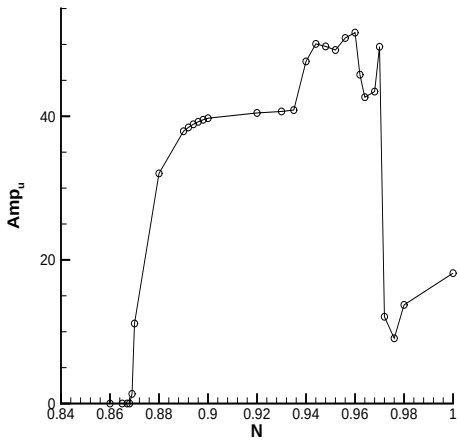

Figure 4: Amplitude of velocity u vs. N.

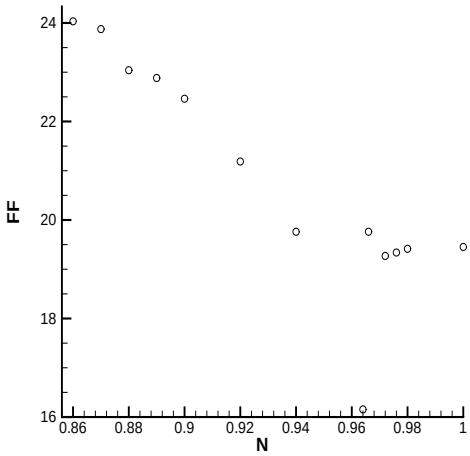

Figure 5: Fundamental frequency of periodical motion vs. N.

can be drawn from Fig. 3. The first is the appearance of a simple self-sustained oscillation, i.e., the sinusoidal behavior, with the FF equal to about 24.033. The second is that the fluctuation of u (or v) is quite small (of order of 10^{-4}), which is because the main structure in the cavity is unchangeable except the periodical variation of small eddies near the top left corner and bottom right corner. As N increases, the self-sustained oscillatory flow with increasing oscillatory amplitudes and decreasing oscillatory FF are obtained. Fig. 4 shows the change of amplitude parameter A_{mp} vs N, where A_{mp} is defined as $A_{mp}=\max[u(t)]-\min[u(t)]$, where $\max[u(t)]$ and $\min[u(t)]$ denote the maximum and the minimum values of $u(t)$, respectively.

When N reaches 0.87, the amplitude has a sudden change as observed in Fig. 4, which means a new flow pattern appears in the flow fields. There appear new FFs in the flow fields, which are about $FF=23.876$, $FF2=47.752$ (the double FF) and $FF3=71.628$ (the triple FF). With N increase to 0.88, a new FF, FF4 (quadruplex FF), appears which corresponds to $FF=23.040$ except for $FF2$, $FF3$, which can be found in Fig. 6. Meanwhile the trajectory in phase space also changes to different flow patterns. Such flow patterns cover the range of buoyancy ratio from N_{11} to N_{12}. Table 4 with checkmarks denotes existence of multiple FFs for different values of N. It can be found that the values of FF decrease gradually but slowly for $0.86\leq N\leq 1$. However, no more higher harmonics were observed in the interval (N_{11},N_{12}). Fig. 5 shows that the values of FF decrease with increasing N in the interval (N_1,N_{12}).

A new flow pattern, chaotic flow, appears in the enclosure for $N\in(N_{12},N_{13})$. Fig. 7 shows that there exists an obvious FF, which coexists with the subharmonics and high harmonics and many background noises. The frequency spectrum characteristic demonstrates that the flow is a kind of chaotic motion. Fig. 4 indicates that the amplitude of velocity u reaches the maximum value in this case.

Fig. 4 also shows that the amplitude decrease quickly for $N>N_{13}$, which indicates

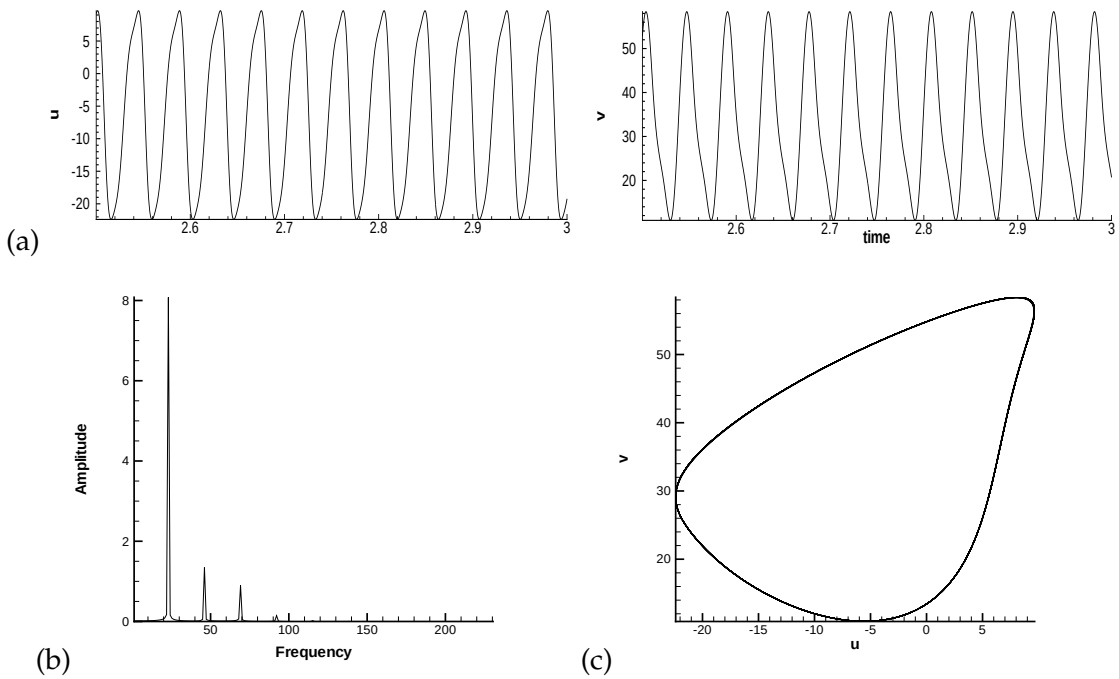

Figure 6: Computed enclosure flow at $N=0.88$. (a) u and v as a function of time; (b) Fourier frequency spectrum of the u velocity; (c) phase-space trajectories of v vs. u.

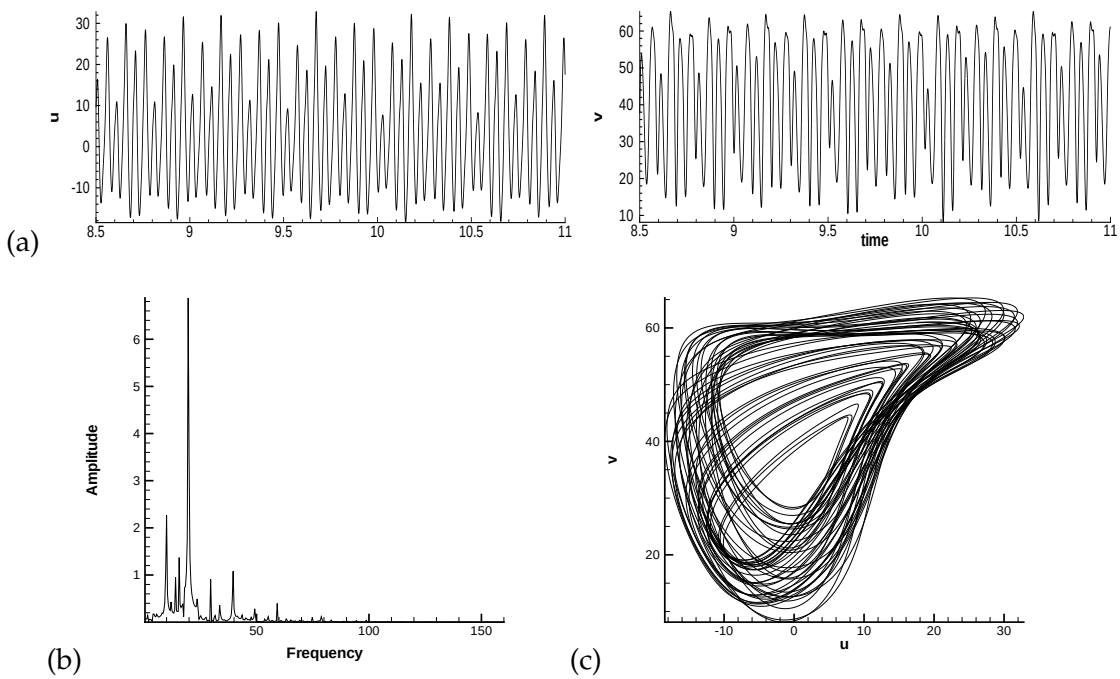

Figure 7: Computed enclosure flow at $N=0.944$. (a) u and v as a function of time; (b) Fourier frequency spectrum of the u velocity; (c) phase-space trajectories of v vs. u.

Table 4: Fundamental frequency and its multiple frequencies for N with periodical motion, FF, $FF2$, $FF3$, $FF4$, $FF5$, $FF6$ denote respectively, fundamental frequency, double FF, triple FF, quadruplex FF, quintuple FF and sextuple FF.

N	FF	FF2	FF3	FF4	FF5	FF6
0.86	24.033	-	-	-	-	-
0.87	23.876	✓	✓	-	-	-
0.88	23.040	✓	✓	✓	-	-
0.89	22.883	✓	✓	✓	-	-
0.90	22.462	✓	✓	✓	-	-
0.92	21.187	✓	✓	✓	-	-
0.94	19.761	✓	✓	✓	-	-
0.964	16.154	✓	✓	✓	-	-
0.966	19.761	✓	✓	✓	-	-
0.972	19.271	✓	✓	✓	-	-
0.976	19.340	✓	✓	✓	✓	-
0.98	19.415	✓	✓	✓	✓	-
1.0	19.453	✓	✓	✓	✓	✓

that the flow pattern returns to the periodic flow in enclosure. It is necessary to point out that the flow is periodic when $N\in(N_{13},N_{14})$ as the buoyancy increases. This seems quite strange, because the translation of the flow pattern is rapid within a very small interval. Fig. 8(a) shows that the time-evolution of the velocity components u and v is more complicated than that in $N\in(N_{11},N_{12})$. Fig. 8(b) reveals that there exist subharmonics and higher multiple FF in the flow, while Fig. 8(c) indicates that the flow is periodical.

Now increase N further. The flow turns into a new pattern, i.e., quasi-periodic motion, for $N\in(N_{14},N_{15})$. Fig. 9 shows some details of such motion. With increasing values of N, the flow return to the periodic flow with addition of a new FF, FF5 (quintuple FF) for $N\in(N_{15},1)$. Fig. 10 demonstrates such typical flow structure. The values of FF and A_{mp} of u variable can be found separately in Table 4 and Fig. 4, which indicate that the values of FF and the amplitude increase with increasing N in this interval. Fig. 11(b) shows that a new FF, FF6 (sextuple FF) adds to the flow, which indicates that the flow pattern has a significant change. Fig. 11(c) shows that the phase-space trajectories are also obviously different from the former ones.

The general trend of the value of FF in the interval $(N_1,1)$ decreases firstly and then increases slightly according to Fig. 5 and Table 4, which is as same as the trend of A_{mp} of u. Table 4 presents the value of FF for different N and its multiple frequencies within the periodical flow region. It is found that when $N\leq 1$, there appears sextuple FF, FF6, in the flow except for FF, FF2, FF3, FF4, FF5. That is a typical process of period doubling. Except for the high harmonics, there are subharmonics turning up in the flow when $N=0.964$ as show in Fig. 8. Table 4 also indicates that the periods increase generally, vs N for the periodic flow, except in the interval (N_{13},N_{14}) where the periods appear a large jump.

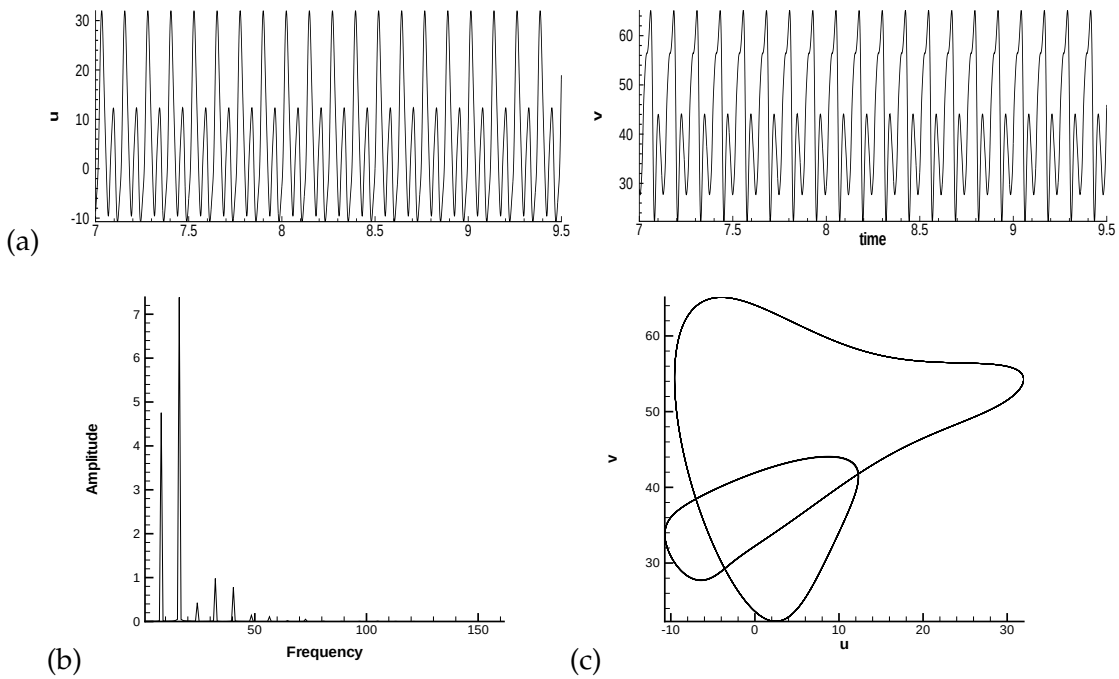

Figure 8: Computed enclosure flow at $N=0.964$. (a) u and v as a function of time; (b) Fourier frequency spectrum of the u velocity; (c) phase-space trajectories of v vs. u.

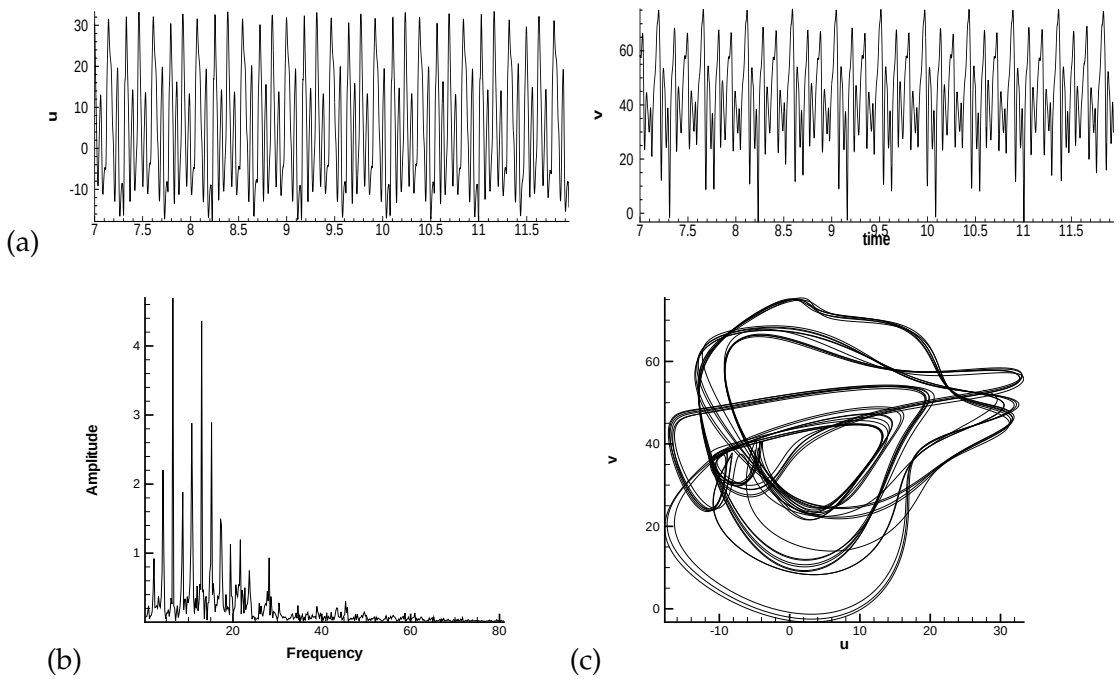

Figure 9: Computed enclosure flow at $N=0.970$. (a) u and v as a function of time; (b) Fourier frequency spectrum of the u velocity; (c) phase-space trajectories of v vs. u.

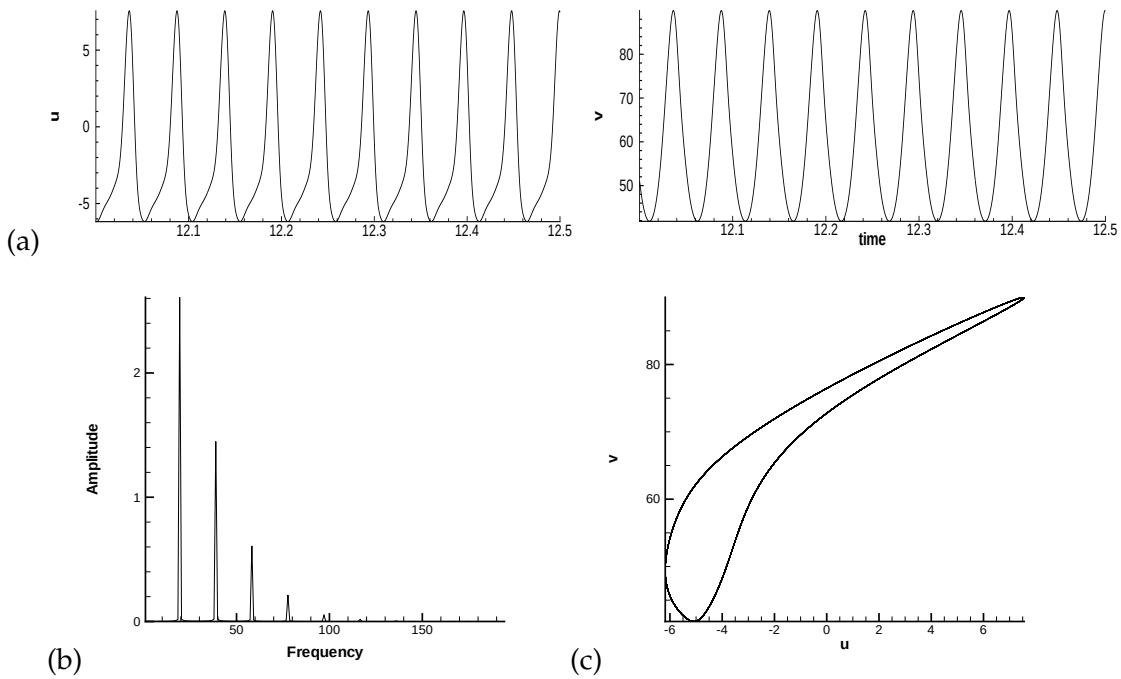

Figure 10: Computed enclosure flow at $N=0.980$. (a) u and v as a function of time; (b) Fourier frequency spectrum of the u velocity; (c) phase-space trajectories of v vs. u.

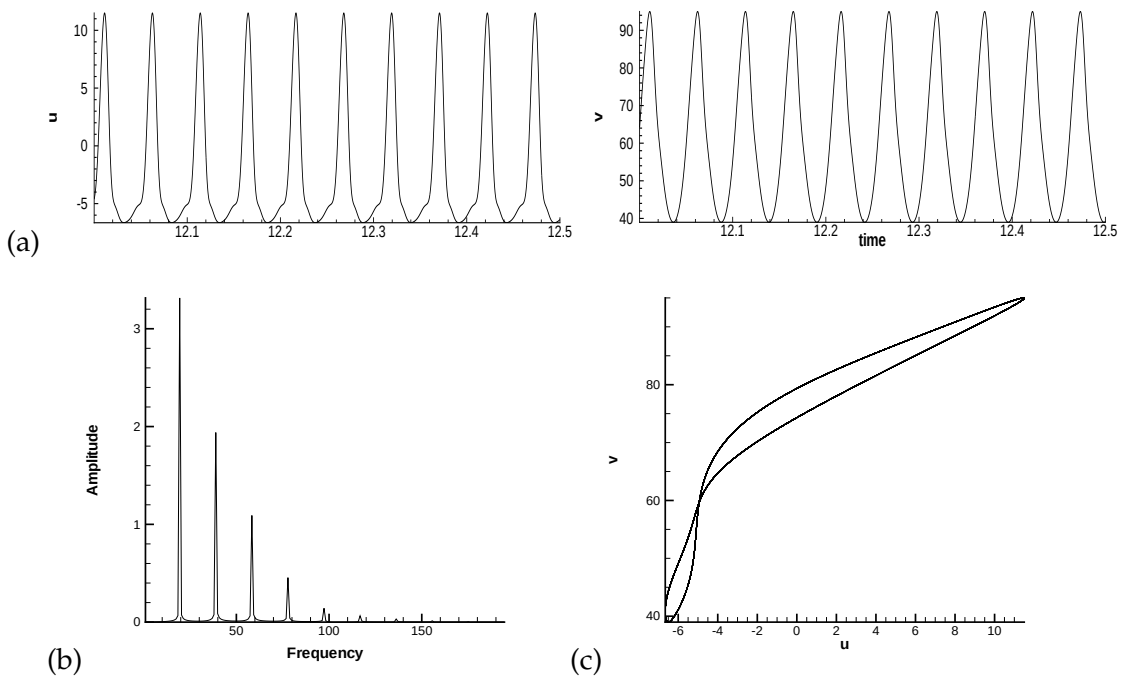

Figure 11: Computed enclosure flow at $N=1.0$. (a) u and v as a function of time; (b) Fourier frequency spectrum of the u velocity; (c) phase-space trajectories of v vs. u.

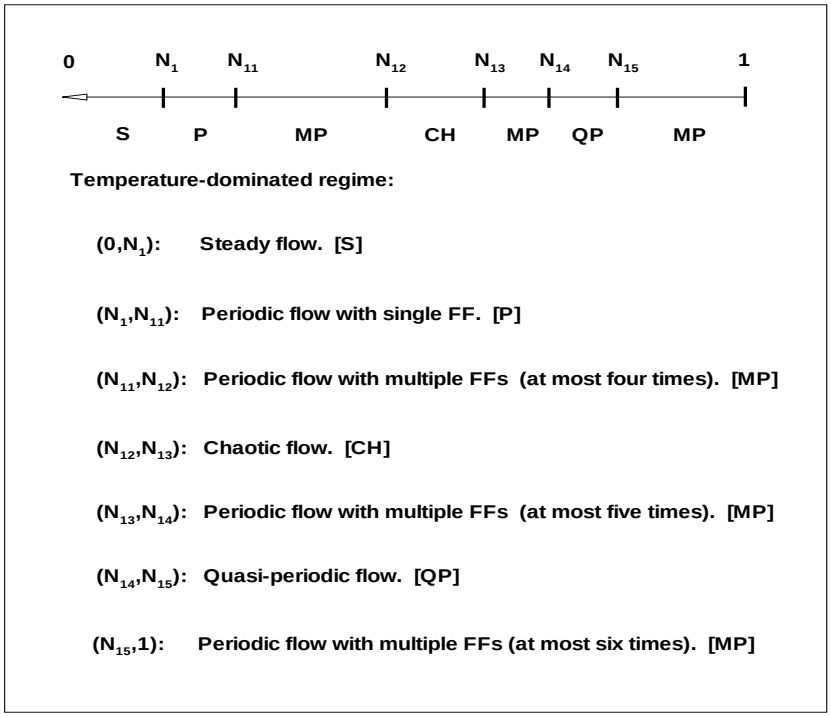

Figure 12: A schematic description about the complex transition in the enclosure flow.

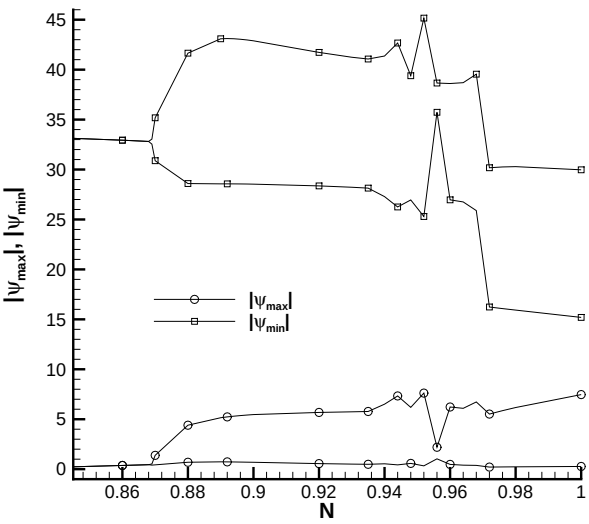

Figure 13: Bifurcation diagrams of thermal and compositional recirculations.

To have a better understanding of such complex transition structure, Fig. 12 demonstrates a schematic description. Fig. 13 illustrates the bifurcation diagrams of the thermal and compositional recirculations. The curls in the plots are not so smooth for $N \in$

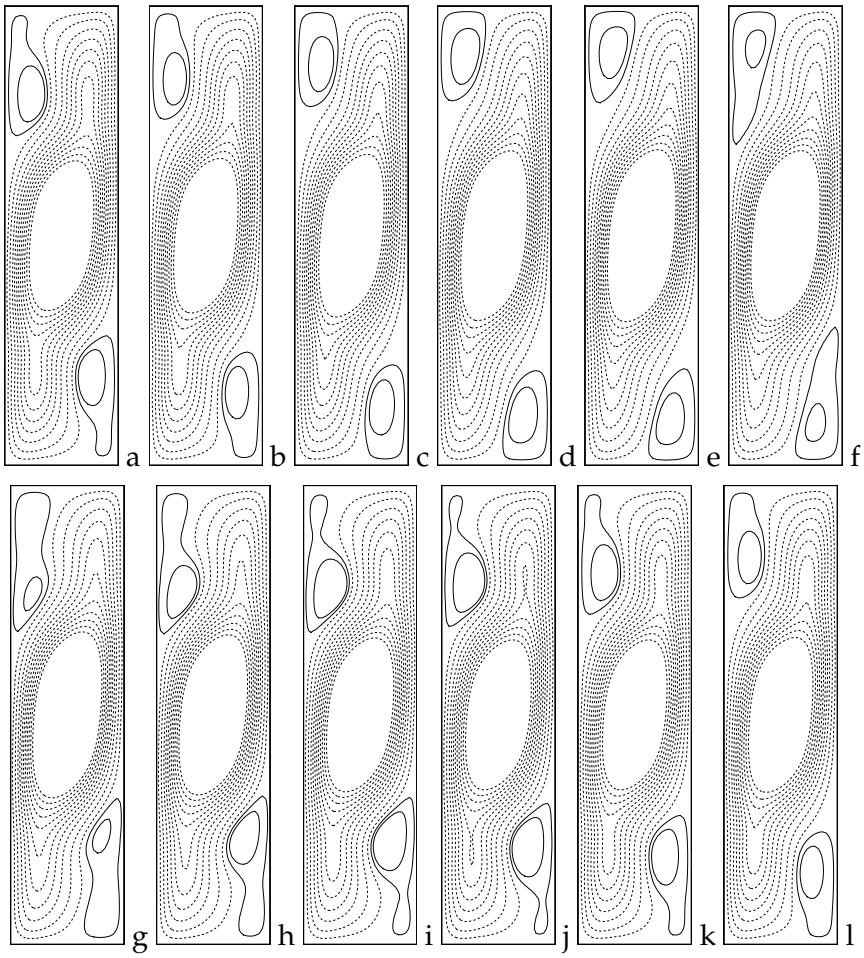

Figure 14: Time history of streamline contours for $N=0.87$. Solid lines: counter-clockwise; dashed lines: clockwise.

(N_{12},N_{13}) where the chaos dominated the enclosure. Such fluctuation indicates the rapid changes in the flow with increasing buoyancy.

As Quon [9] pointed out that the temperature and concentration effect tend to counteract for $N\in(0,1)$ and $N\in(1,2)$ only when the Lewis number $Le=1$ and the Rayleigh number is sufficiently small. Although $L=2$ in the present paper, the flow pattern should be in some degree similar in the intervals $(0,1)$ and $(1,2)$. It will be interesting to further study the problem for $N\in(1,2)$. This remains to be a future research topic.

4.2 Fields structure of periodic flow

In this part, the flow structure of the periodic flow is investigated. Fig. 14 shows that there is only a large primary vortex in the middle part of the enclosure and two small

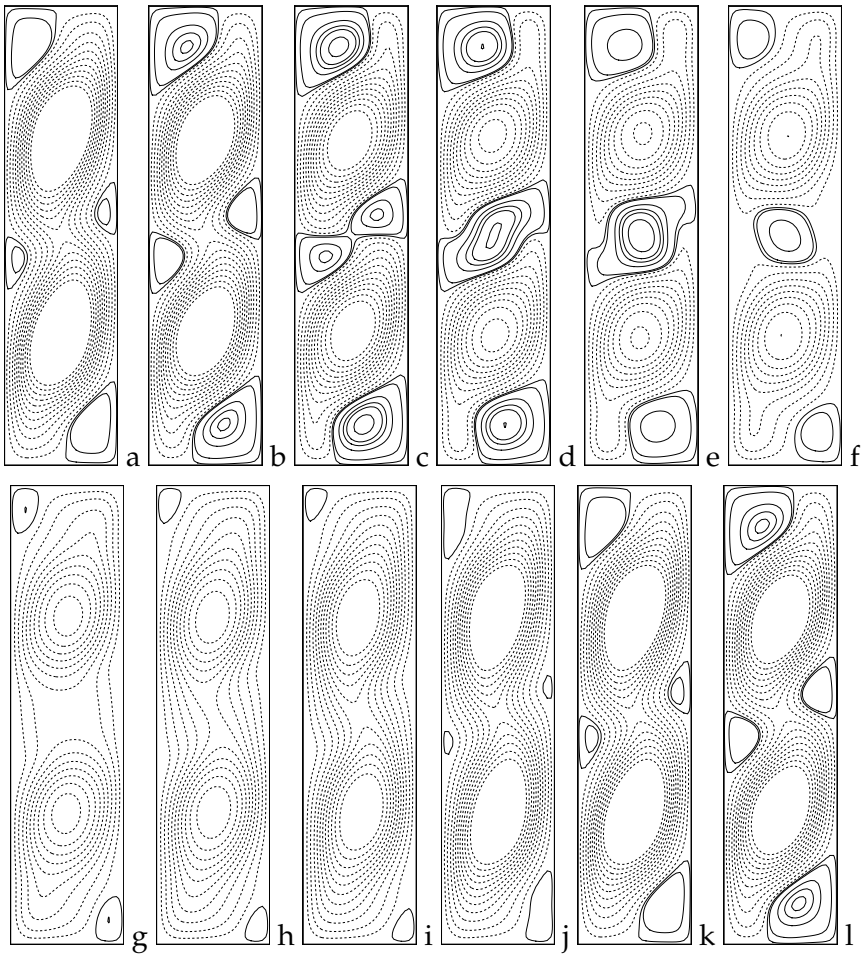

Figure 15: Time history of streamline contours for $N = 0.98$. Solid lines: counter-clockwise; dashed lines: clockwise.

secondary vortexes respectively in top left corner and bottom right corner. Fig. 14(a) to (k) (or (b) to (l)) demonstrate a complete periodic evolution. The non-dimensional time interval is 0.00419. Fig. 14(k) and (l) are similar to (a) and (b), respectively. The changes of the flow fields mainly come from the two secondary vortex with time advancing, while the primary vortex only changes slightly.

However, if $N=0.98$, the flow structure turns into very complex. Fig. 15 indicates that the flow pattern turns into multi-vortex structure. Fig. 15(a) to (k) (or (b) to (l)) demonstrate a completed periodic evolution. The non-dimensional time interval is 0.00515. Fig. 15(k) and (l) are similar to (a) and (b), respectively. Two primary vortexes have remarkable change as well as small vortexes appearing in the top, bottom and middle part of the enclosure. So there exist multi-scale and multi-frequency oscillation motion in the enclosure.

In addition, the flow fields are symmetrical in the spatial structure in the above two cases. As for comparison, if the flow are quasi-periodic and chaotic, the flow fields become asymmetrical.

5 Conclusions

The transition process is studied numerically in a rectangular enclosure subject to the opposing horizontal thermal and compositional buoyancy.

• Firstly, there exist multi flow patterns in the rectangular enclosure with $A=4$ for $0\leq N\leq 1$, $Ra_T=10^5$, $Pr=1$ and $Le=2$. The flow structure can be steady, periodic, quasi-periodic and chaotic.

• Secondly, the present transition contains five processes: 1) the steady flow to the periodic flow via supercritical Hopf bifurcation; 2) the periodic flow to the chaos via a series of period doubling; 3) the chaos back to the periodic flow; 4) the periodic flow to the quasi-periodic flow; 5) the quasi-periodic flow back to the periodic flow.

This complex flow is a result of a strong nonlinear system with multi-procedure coupling and multi-physics modeling.

Acknowledgments

The authors thank Shanghai Supercomputer Center (SSC) for providing computer time. This work was supported by National Natural Science Foundation of China (Grant Nos. 10632050, 10502052).

References

[1] H. M. Stommel, Thermohaline convection with two regimes of flow, Tellus,13(2) (1961), 224-230.

[2] P. Welander, Thermohaline effects in the ocean circulation and related simple models, Large-scale Transport Processes in Oceans and Atmosphere, NATO ASI Series, Reidel (1986), 163-304.

[3] F. Bryan, High-latitude salinity effects and inter hemispheric thermohaline circulation, Nature, 323 (1986), 301-304.

[4] J. W. Lee and J. M. Hyun, Double-diffusive convection in a rectangle with opposing horizontal temperature and concentration gradients, Int. J. Heat Mass Transfer, 33(8) (1990), 1619-1632.

[5] J. W. Lee and J. M. Hyun, Technical notes: Double-diffusive convection in a cavity under a vertical solutal gradient and horizontal temperature gradient, Int. J. Heat Mass Transfer, 34(9) (1991), 423-2427.

[6] K. Hanjalic and R. Musemic, Modeling the dynamics of double-diffusive scalar fields at various stability conditons, Int. J. Heat Mass Transfer, 18 (1997), 360-367.

[7] T. Bergman, F. Incropera and R. Viskanta, A differential model for slat-stratified, double-diffusive systmes heated from below, Int. J. Heat Mass Transfer, 28 (1985), 779-788.

[8] T. Bergman and F. Incropera and R. Viskanta, Correlation of mixed layer growth in a double-diffusive, salt-stratified system heated form below, Int. J. Heat Mass Transfer, 108 (1986), 206-211.

[9] C. Quon and M. Chill, Multiple equilibria in thermosolutal convection due to sal-flux boundary conditions, J. Fluid Mech., 245 (1992), 449-483.

[10] C. Quon and M. Chill, Multiple equilibria stable oscillation in thermosolutal convection at small aspec ratio, J. Fluid Mech., 291 (1994), 33-56.

[11] T. Nishimura, M. Wakamatsu and M. M. Alexandru, Osillatory double-diffusive convection in al rectangular enclosure with combined horizontal tmperature and concentration gradients, Int. J. Heat Mass Transfer, 41(11) (1998), 1601-1611.

[12] S. Garcia, The lid-driven square cavity flow: From stationary to time periodic and chaotic. Commun. Comput. Phys., 2 (2007), 900-932.

[13] N. Tsitverblit, Bifurcation phenomena in confined thermosolutal convection with lateral heating: commencement of the double-diffusive region, Phys Fluids, 7(4) (1995), 718-736.

[14] E. Papanicolaou and V. Belessiotis, Double-diffusive naturnal convection in an asymmetric trapezoidal enclosure: unsteady behavior in the laminar and the trululent-flow regime, Int. J. Heat Mass Transfer, 48 (2005),191-209.

[15] Y. Masuda, M. Yoneya, A. Suzuki, S. Kimura and F. Alavyoon, Numerical analysis of double-diffusive convection in a porous enclosure due to opposing heat and mass fluxes on the vertical walls — why does peculiar oscillation occur? Int. J. Heat Mass Transfer, 51 (2008) 383-388.

[16] T. Nishimura, T. Imoto and M. Wakamatsu, A numerical study of the structure of double-dffusive natural covection in a square cavity, Proc. of 4th ASME/JSME Thermal Eng Conference, 1 (1995), 193-200.

[17] T. Nishimura, T. Imoto and M. Wakamatsu, A numerical study of the structure of double-dffusive natural covection in a rectangular enclosure filled with binary gas, Trans. JSME Ser B, 62 (1996), 271-277.

[18] K. Sundaravadivelu and P. Kandaswamy, Double diffusive nonlinear convection in a suqare cavity, Fluid Dynamics Research, 27 (2000), 291-303.

[19] S. K. Lele, Compact finite difference schemes with spectral-like resoution, J. Comput. Phys., 103 (1992), 16-42.

[20] C. W. Shu and S. Osher, Efficient implementation of essentially non-oscillatory shock-capturing schemes, J. Comput. Phys., 77 (1988), 439-471.

[21] L. Gamet, F. Ducros, F. Nicoud and T. Poinsot, Compact finite difference schemes on non-uniform meshes. Application to direct numerical simulations of compressible flows, Int. J. Numer. Meth. Fluids, 29 (1999), 159-191.

[22] D. X. Fu and Y. W. Ma, A high-order accurate difference scheme for complex flow fields, J. Comput. Phys., 134 (1997), 1-15.

[23] X. Liang, Z. F. Tian, High order method for solving unsteady incompressible Navier-Stokes equations, WSEAS Trans Math., 5(6) (2006), 640-647.

[24] M. M. Gupta, High accuracy solution of incompressible Navier-Stokes equations. J. Comput. Phys., 93 (1991), 343-359.

[25] M. Li, T. Tang and B. Fornberg, A compact fourth-order finite-difference scheme for the steady incompressible Navier-Stokes equations. Int. J. Numer. Meth. Fluids, 20 (1995), 1137-1151.

[26] Z. F. Tian and Y. B. Ge, A fourth-order compact finite difference scheme for the steady stream function-vorticity formulation of the Navier-Stokes/Boussinesq equations. Int. J. Numer. Meth. Fluids, 41(5) (2003), 495-518.

[27] J. Y. Choo and D. H. Schultz, A high order difference method for the steady state Navier-Stokes equations. Computers Math. Appl., 27(11) (1994), 105-119.
[28] A. M. Morega and T. Nishimura, Double-diffusive convection by a Chebyshev collocation method, Technology Reports, Yamaguchi University, 5(1996), 259-276.
[29] D. Gobin and R. Bennacer, Double-diffusion in a vertical fluid layer: onset of the convective regime, Phys. Fluids A, 6 (1994), 59-67.